Robust Surface Nano-Architecture by Alkali−Carboxylate Ionic Bonding
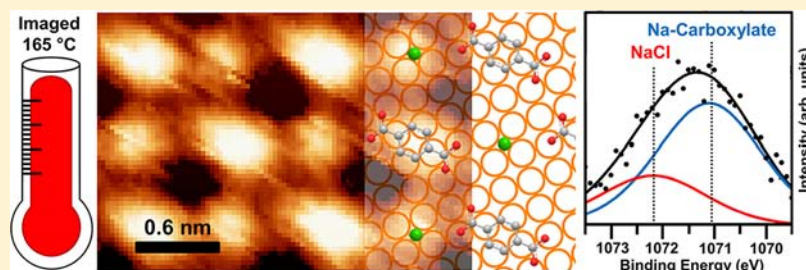
Daniel Skomski,[†] Sabine Abb,[†,‡] and Steven L. Tait*,[†]

[†]Department of Chemistry, Indiana University, Bloomington, Indiana 47405, United States
[‡]University of Tübingen, Auf der Morgenstelle 18, 72076 Tübingen, Germany

S *Supporting Information*

ABSTRACT: Ionic bonding in supramolecular surface networks is a promising strategy to self-assemble nanostructures from organic building blocks with atomic precision. However, sufficient thermal stability of such systems has not been achieved at metal surfaces, likely due to partial screening of the ionic interactions. We demonstrate excellent stability of a self-assembled ionic network on a metal surface at elevated temperatures. The structure is characterized directly by atomic resolution scanning tunneling microscopy (STM) experiments conducted at 165 °C showing intact domains. This robust nanometer-scale structure is achieved by the on-surface reaction of a simple and inexpensive compound, sodium chloride, with a model system for carboxylate interactions, terephthalic acid (TPA). Rather than distinct layers of TPA and NaCl, angle resolved X-ray photoelectron spectroscopy experiments indicate a replacement reaction on the Cu(100) surface to form Na−carboxylate ionic bonds. Chemical shifts in core level electron states confirm a direct interaction and a +1 charge state of the Na. High-temperature STM imaging shows virtually no fluctuation of Na−TPA island boundaries, revealing a level of thermal stability that has not been previously achieved in noncovalent organic-based nanostructures at surfaces. Comparable strength of intermolecular ionic bonds and intramolecular covalent bonds has been achieved in this surface system. The formation of these highly ordered structures and their excellent thermal stability is dependent on the interplay of adsorbate−substrate and ionic interactions and opens new possibilities for ionic self-assemblies at surfaces with specific chemical function. Robust ionic surface structures have potential uses in technologies requiring high thermal stability and precise ordering through self-assembly.

INTRODUCTION

The increasing importance of organic-based nanotechnology requires new strategies to program structure and function in molecular architectures with atomic precision at surfaces. Existing "top-down" methods for the production of structures on the nanoscale are expected to reach their limits soon.[1] Surface-assisted self-assembly is a "bottom-up" alternative through which atomic control of nanostructures can be achieved, as in natural biological systems. Organic self-assembly at surfaces holds promise for large-scale fabrication of functional nanostructures[2−5] for use in chemical sensors, protective coatings, molecular electronics, and organic photovoltaics.[6,7] However, most studies in this field employ relatively weak binding; examples of highly robust organic nanostructures are lacking. In organic-based solar devices, robust architectures may reduce unwanted interfacial effects, like interfacial diffusion,[8] and improve operational lifetimes during high-temperature stress conditions of full sun illumination.[9] The

construction of robust, self-assembled nanostructures is a key requirement for long-term device performance and reliability.

Much of the focus in surface-assisted self-assembly has been on the use of van der Waals and hydrogen-bonding interactions, which have yielded many examples of highly ordered surface structures, with relatively weak interactions,[3,10,11] sometimes studied at low temperatures. On-surface polymerization through covalent bonding has been used to form strongly bound structures,[12] but these have limitations due to the nonreversibility of the bonding, which can inhibit both long-range ordering during growth and capability for self-repair. Ordering, stability, and self-repair are each key motivations for the use of organic materials to program surface functionality.

Ionic interactions afford a way to achieve functionalized nanostructures at interfaces and have proven highly effective for

long-range ordering.[13] Ionic interactions provide thermal stability in bulk devices[14] as well as in protein structures around 100 °C.[15] Work has shown that supramolecular systems assembled via ionic interactions are less susceptible to problems of interfacial diffusion than those constructed using van der Waals or hydrogen-bonding interactions.[16] However, ionic interactions at surfaces are not yet well understood. One study of alkali metals examined structures formed by guanine and potassium, though formation of a strong ionic bond was not observed, and structures were stable only at cryogenic temperatures.[17] Two studies have presented self-assembled ionic networks at surfaces constructed from alkali metal cations and anionic organic species.[13,18] While gas-phase alkali metal atoms can be adsorbed directly onto surfaces to construct ionic networks under ultrahigh vacuum conditions,[13] the very high reactivity of said gaseous species[19] may make them unsuitable for use in higher pressure environments. An alternative method for self-assembly of ionic species involves the reaction of a common, low cost, and relatively inert sodium salt, sodium chloride, with nitrile species on the metallic surface to yield highly ordered nanoscale structures.[18] An on-surface reaction of the salt with the common carboxyl functional group had not been illustrated until now.

Questions remain as to the stability of ionic structures at surfaces, especially whether metal surface screening will weaken the interaction and, conversely, whether concurrent chemisorptive bonds could add stability to the ionic structures. In prior work, only low stability on metal surfaces at room temperature has been reported.[13] It is known that ionic interactions are weakened in solution media, but are very strong in the gas phase.[20] The behavior of the metal surface may, in some cases, screen the interaction and weaken the ionic bonds. New strategies are necessary to take advantage of the potential strength of ionic bonds in the self-assembly of robust nanostructures at surfaces.

In this paper, we report thermally robust ionic nanostructures at a metal surface. Highly ordered, self-assembled domains are intact and stable at 165 °C, as shown directly by atomic resolution, high-temperature scanning tunneling microscopy. The on-surface reaction involves a highly economical and safe reactant, sodium chloride, with carboxylate species to produce self-assembled architectures by ionic bonding. Self-assembly of carboxyl species, such as terephthalic acid here, is very important because of the prevalence of this functional group in energy-related applications.[21−24] We suggest that the long-range self-assembly of a highly robust organic structure at solid surfaces requires both strong ionic adsorbate−adsorbate interactions as well as strong metal−organic chemisorption to the surface. We illustrate that metal−organic and ionic interactions can work in concert to induce self-assembly of a highly robust organic nanostructure (such as the sodium−terephthalate, Na−TPA, α phase) with atomic precision. The Na−TPA ionic structures on Cu(100) studied here exhibit excellent thermal stability, maintaining their atomic organization at 165 °C. Above this temperature, scission of intramolecular C−C bonds in the terephthalate suggests that intermolecular ionic and intramolecular covalent interactions can be comparable in strength in nanoscale self-assemblies at metal surfaces.

■ RESULTS AND DISCUSSION

As a model system for the study of highly robust, self-assembled nanostructures by ionic bonding, we investigate the self-

assembly of a carboxylate building block ("TPA") with cationic species (Na ions, formed by a surface reaction with NaCl) on the copper (100) surface in ultrahigh vacuum conditions. TPA is a model carboxylate building block that is used as a self-assembled adhesion layer on a variety of surfaces[25−27] and forms a strong metal−organic bond to the copper surface[28] after deprotonation of its acid groups.[29] NaCl has previously been investigated for use as an insulating layer on surfaces[30−32] but is used as a reactant to generate Na ions in this study. Na ions possess higher charge density than other alkali metal cations and should form strong ionic bonds.

Surface Reaction of NaCl and TPA. X-ray photoelectron spectroscopy experiments provide evidence for the formation of an ionically bound Na−TPA structure. New chemical interactions upon addition of TPA to NaCl on the Cu(100) surface are evidenced by a shift in the Na 1s core level to lower binding energy, as shown in the XP spectra in Figure 1. NaCl
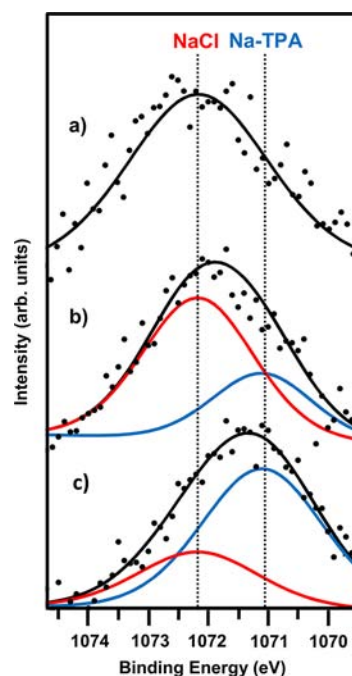
Figure 1. Sodium 1s XPS peak of: (a) low (submonolayer) coverage of NaCl on Cu(100) with annealing at 130 °C; (b) then with addition of submonolayer coverage of TPA; and (c) annealed again at 130 °C.

on the Cu(100) surface annealed at 250 °C gives a single Na 1s peak at 1072.2 eV, consistent with prior experiments.[33] After addition of TPA, the Na 1s peak envelope shifts to 1072.0 eV, due to a new chemical state for Na at lower binding energy. The shift becomes more pronounced upon annealing at 130 °C, shifting to 1071.4 eV. In the latter two experiments (Figure 1b,c), the Na 1s peak is fit well by two components: The first is constrained in energy to match the trace in Figure 1a (1072.2 eV), corresponding to Na in NaCl. The second component (1071.1 eV) is at the same energy in Figure 1b,c and corresponds to a new chemical state for Na, observed after deposition of TPA. The shift in the Na 1s binding energy due to addition of TPA implies the presence of new interactions that are not observed if each species is deposited onto Cu(100) by itself. No significant difference is observed in either the C 1s or O 1s XPS peaks for the NaCl and TPA mixture compared to TPA on Cu(100) alone, when both have been annealed. This is

likely due to the fact that the deprotonated TPA is already in an anionic state and forming a significant chemical bond to the surface.

The changes in the chemical environment of Na after TPA deposition support the idea that the TPA and Na mix rather than forming distinct, noninteracting surface structures, i.e., new interactions between Na and TPA become possible if both exist on the Cu(100) surface. Notably, the fitted peak at the lower binding energy, associated with the Na−TPA interaction, grows substantially after subjecting the surface to an annealing treatment at 130 °C (Figure 1c). This change is likely due to an increase of the Na−TPA interaction; no such change is observed for identical treatment of the NaCl on Cu(100) in the absence of TPA.

Analysis of the Na KLL Auger peak indicates that the Na retains a +1 charge state upon reaction with the TPA. While overlap has been shown to exist in the Na 1s peak location between charged and noncharged sodium states, the difference in peak position is significant for the Na KLL peak. On the copper surface with both TPA and NaCl, the Na KLL kinetic energy peak is located at 990 eV (Figure 2). The peak location
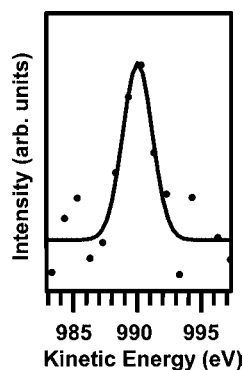

Figure 2. Sodium KLL Auger peak after addition of TPA to NaCl on Cu(100) and annealing. KLL peak position is consistent with Na in +1 charge state.

is in excellent agreement with the case when Na has a +1 charge, as in the bulk NaCl form where the peak is located at 990.0−990.3 eV.[34] The peak location is not in agreement with Na possessing a zero charge, as in its metallic form, when the peak is located at 994.3 eV.[34]

Two possibilities were investigated to account for the perturbation of the chemical state of sodium due to new interactions with TPA: first the formation and interaction of distinct layers of a NaCl/TPA interface and second a chemical reaction between TPA and NaCl, leading to the formation of integrated networks of these surface species. Angle-dependent XPS measurements were used to obtain depth information near the surface.[35] XPS measurements show that there is little variation in the ratio of the C 1s to Na 1s XPS peak areas, as the angle between the sample and the detector is varied (Figure 3). A model based on the Beer−Lambert relationship[35] demonstrates the variation in C:Na intensity ratio that one would expect for layered growth: either TPA growth on top of NaCl islands (red) or NaCl growth on top of TPA (blue). Such a model stipulates that, with a NaCl-rich layer on top of (underneath) a carbon-rich layer, a significant decrease (increase) in the C 1s to Na 1s peak area ratio would be expected as the takeoff angle is increased and surface sensitivity is enhanced. However, our experimental data show little change
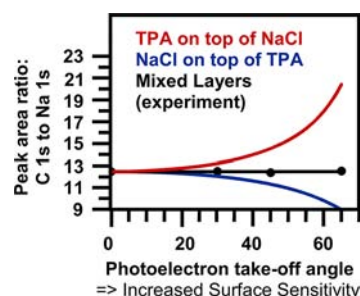

Figure 3. The change in the ratio of the C 1s and Na 1s XPS peak area, on a Cu(100) surface onto which TPA was deposited first and then NaCl, as the angle between the normal of the sample and the line of sight of the electron energy analyzer (takeoff angle) is increased and surface sensitivity is enhanced. The result of a simplified theoretical model is also shown, which assumes formation of largely distinct layers of NaCl on top of TPA and vice versa.

in the C 1s to Na 1s ratio with varying takeoff angle, indicating that C and Na are mixed in the overlayer. This result is independent of the order of deposition of NaCl and TPA to the Cu(100) surface.

The replacement reaction of TPA with NaCl is further confirmed by XPS analysis of the Cl 2p intensity, which decreases significantly during the surface reaction. Before deposition of TPA onto a Cu(100) surface covered with NaCl, STM images show islands with rectangular edges. These islands are three-dimensional NaCl structures, as was determined in a prior low-temperature study.[31] An indicator of the disruption of the intact NaCl phase upon addition of TPA to the surface is that NaCl islands with rectangular edges are still observed if a large excess of NaCl is present on a TPA/NaCl surface (see Figure S1 for an example) but are not seen at all if an excess of TPA is present. Furthermore, after addition of TPA to NaCl and annealing at 130 °C, a decrease in the Cl 2p XPS peak area of 47% can be seen as well as a shift in the peak maximum from 199.2 to 198.6 eV (Figure 4). Prior studies have reported desorption of copper chloride species[36] and diffusion of Cl into the bulk lattice,[37] with the latter mechanism likely accounting for the residual Cl 2p XPS signal in our experiments. (For further discussion, see Supporting Information.)
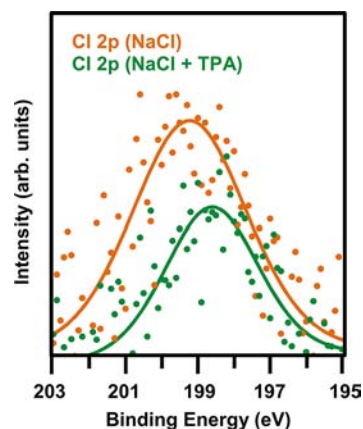

Figure 4. Chlorine 2p XPS photoelectron peak. Upper trace: Annealed NaCl of submonolayer coverage on Cu(100). Lower trace: Annealed NaCl of submonolayer coverage on Cu(100), after addition of TPA and annealing again at 130 °C.

While the reaction of NaCl and TPA to form an ionic sodium terephthalate compound is not favored in solution, the complete and irreversible, surface-catalyzed deprotonation of TPA, in the absence of Na, is of importance in enabling the reaction at the metal surface. Charge transfer from the Cu surface must occur to enable deprotonation of the carboxylic acid groups.[38,39] Charge transfer from Cu to other organic species has been shown to be an important component in supramolecular self-assembly at surfaces.[40,41] Once deprotonated, TPA abstraction of Na from NaCl must necessarily occur. The dissolution of transition-metal bilayer islands by carboxylate species has been shown previously,[42] though in the present case, dissolution of an alkali compound is observed. Segregation of Na and Cl ions into a Na-rich underlayer and a Cl-rich overlayer in the absence of TPA, as suggested by preliminary angle-resolved XPS data, may play a role in facilitating the dissolution of the multilayered NaCl islands by TPA. Furthermore, copper chloride intermediates are known to form on the copper surface[43] and possess greater lattice energies than NaCl in the bulk form.[44] The intermediates may favorably alter the thermodynamic landscape of the reaction as compared to the solution case, although additional studies would be required to conclusively determine this.

Structure of New Na−TPA Ionic Compound. STM images of a Cu(100) surface with submonolayer coverages of TPA and NaCl were acquired and show the formation of hybrid structures made up of TPA and Na. The same structures are observed regardless of whether TPA or NaCl is deposited first. The structure shown in Figure 5, hereafter referred to as the α
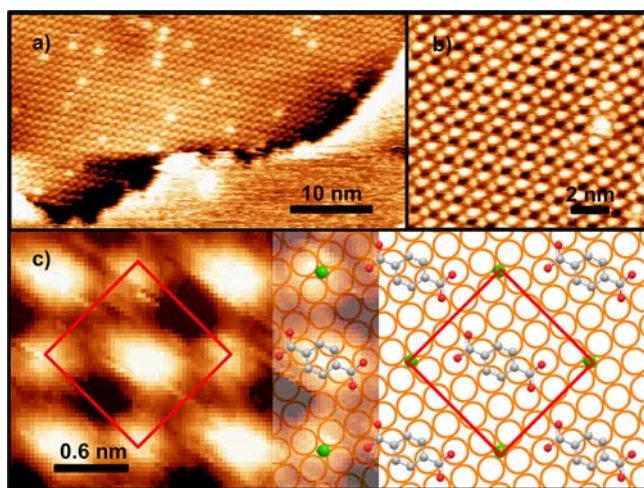

Figure 5. STM images of the Cu(100) surface with TPA and NaCl, after annealing to 160 °C. (a) Part of a large island made up of the Na−TPA α phase. (b) Molecular and atomic resolution of the island in (a). (c) Zoom in of (b), with a schematic representation of the orientation of the Na−TPA α phase on the copper surface.

phase, is the most commonly observed structure after deposition at room temperature and is the dominant structure increasing in fractional surface coverage after prolonged annealing treatments. Of note is that a difference in contrast and size is seen between different dots in the STM image. One dot appears as a sphere, and the other appears higher in the STM topography and is elongated in one direction. The presence of two distinct dots in the STM image is indicative of the presence of two different species in the structure. Of course, the size of particular species is only one factor that impacts the

images that are produced, and more accurately, it is the convolution of the local density of states of the surface and of the tip that ultimately produces the final image. For example, the Na cations appear in the STM images to be nearly as large as the TPA molecules, while in reality they should be small compared to the TPA. In one experiment, tip modification, likely due to adsorption of some species to the tip, caused a change in the density of states of the tip such that the two surface species appeared with similar contrast in the STM images (Figure S2). In situ tip cleaning in many different experiments regularly yields images like those in Figure 5.

We can consider the electrostatic potential map of the deprotonated form of TPA to explain what atoms may be involved in the formation of the observed phase and deduce the formation of a Na−TPA structure. The carboxylate groups on opposite ends of the deprotonated form of TPA are negatively charged, leading to an attractive electrostatic interaction to the Na cations. The crystal structure of disodium terephthalate powder was previously studied, and Na was said to adopt a trigonal prismatic coordination.[45] While that solid crystal study found the expected 2:1 stoichiometric ratio of Na^+:TPA^{2-} to maintain charge neutrality, a lower ratio may be accommodated in surface studies by charge screening and the presence of image charges in the conductive copper surface. Indeed, charge compensation afforded by the metallic copper surface accounts for the ability of negatively charged terephthalate molecules to self-assemble into organized structures of a molecular phase, even at low coverage,[29] or around a singly charged cation in a 1:4 Cs^+:$[-COO^-]$ ratio[13] or the 1:2 Na^+:$[-COO^-]$ ratio observed here.

The alternating features form a periodic structure with square unit cell size of $(10.8 \text{ Å})^2$. The measured structure in STM (distances and angles) agrees with an overlayer structure that is commensurate with the Cu(100) surface, likely an important factor in the robust thermal stability of this system (*vide infra*). A structural model is shown in Figure 5c, where the overlayer basis vectors are $b_1 = 4\,a_1 + 2\,a_2$ and $b_2 = -2\,a_1 + 4\,a_2$. The 11.4 Å distance between identical particles in this model is within 6% of the experimentally determined distance. We suspect that the α phase is commensurate with the Cu(100) surface because the appearance of the features in the pattern is perfectly uniform, i.e., apparently the adsorption sites for each TPA and Na are the same across the structure. The TPA−TPA direction (b_1) is rotated 27° relative to the [011] direction of the Cu surface. Hence, the structures in the STM images may be described as a network of alternating TPA and sodium atoms that adopt a $(2\sqrt{5} \times 2\sqrt{5})\,R27°$ structure relative to the copper surface. In the model shown in Figure 5c, the long molecular axis of TPA is not lined up with the center of Na ions to account for the presence of holes in the overlayer structure and to be consistent with the apparent angle observed in the STM data. It may be that this apparent angled orientation of the TPA, relative to the center of the Na ions, is due to a difference in the interactions of the oxygen atoms: one with the Na cation and the other bonding to a copper atom. The angled orientation of TPA in the ionic structures and its commensurability with the surface serve as an indicator of the complementarity of ionic and metal−organic interactions in this system.

Diversity of Structural Phases. While the Na−TPA α phase is the most common structure on the Cu(100) surface with TPA and NaCl, additional Na−TPA structures are also commonly observed (see Table S1). A clear contrast between

14168

dx.doi.org/10.1021/ja3053128 | *J. Am. Chem. Soc.* 2012, 134, 14165−14171

Na and TPA is obtained in STM images of most of these structures and reveals a 1:1 Na:TPA ratio. The possibility that structures with other ratios exist cannot be ruled out. The great diversity of structural formations is not unexpected when one considers the electrostatic, nondirectional nature of ionic bonding. Indeed, in prior work regarding another alkali metal, Cs, and TPA on Cu(100), various structures were observed, and the flexibility of the involved interactions was deemed to be the cause.[13]

It is possible to increase the fraction of the Na−TPA α phase at the expense of the pure TPA phase by annealing treatments, if sufficient Na is available on the surface. With a submonolayer coverage, islands of the Na−TPA α phase were found to be 100−500 nm^2 in size. After annealing, islands of the Na−TPA α phase were found to be about 700−1700 nm^2 in size. The increase in average size of the Na−TPA α phase is accompanied by a decrease in the overlayer surface area occupied by the pure TPA phase, indicating that the increase in island size is not exclusively due to island ripening, but that there is some growth of new Na−TPA material on the islands. When 15 unique spots were sampled on the surface before and after annealing and account was taken of the structures of islands, TPA islands made up approximately 5% of the area before annealing (compared to approximately 30% occupied by the Na−TPA phase) but only about 1% after annealing. The diffusion of TPA at higher temperatures, allowing for the growth of the Na−TPA α phase and the shrinking of the TPA phase, is consistent with the enhanced shift in the Na 1s XPS peak in Figure 1 after annealing.

The possibility of multilayer formation was considered to account for the diversity of Na−TPA structures. Many molecules,[46] including TPA,[47] have been observed to assume different structures in the first layer than they do in upper layers. Even in submonolayer deposition experiments, multi-layer formation is possible if three-dimensional growth is preferred to layer-by-layer growth. However, TPA has been shown to possess great affinity toward copper surfaces, and completion of the first layer occurs before growth of the second layer.[28] When small amounts of pure TPA (submonolayer coverage) are added to the copper surface and annealed and miniscule amounts of Na are subsequently added, several Na−TPA phases are still observed, along with regions of bare Cu surface, proving that multilayer formation is not responsible for the diversity of phases. Also, XPS results indicate that the absolute surface concentration of molecules does not exceed a monolayer coverage.

Although the relative population of the Na−TPA α phase increased with annealing, it was not possible to completely force the exclusion of the other phases. Even when the surface was cooled gradually after annealing over a period of 12 h, various Na−TPA structures were still observed. It seems that some of the Na−TPA structures are energetically degenerate within the capabilities of the experiment. It needs be emphasized, however, that the Na−TPA α phase is by far the most dominant and accounts for a majority of the area occupied by surface structures.

Thermodynamic Stability of Structures. The thermal stability of the Na−TPA structure can be directly observed using high-temperature STM. Intact Na−TPA islands were imaged by STM at a sample temperature of 165 °C (Figure 6) and were seen to be stable at that temperature over a series of many scans. After annealing at this temperature, XPS measurements show an enhanced Na 1s XPS peak shift,
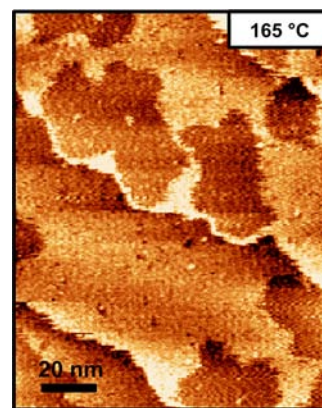

Figure 6. Na−TPA islands imaged with STM at a sample temperature of 165 °C on the Cu(100) surface, with a submonolayer coverage of TPA and NaCl.

indicating further reaction of Na and TPA to create more Na−TPA structure on the surface. Indeed, in one STM experiment, we observed the growth of a Na−TPA island (in real time) during the first several minutes at elevated temperatures (Figure S3). After some further growth of Na−TPA in the first minutes at elevated temperature, the islands are stable for as long as we continue to scan at high temperature. Island shapes remain constant, and virtually no motion of molecules on the island edges can be observed because the Na−TPA bonding is stable at elevated temperatures.

An inability to break up Na−TPA structures at high temperature (165 °C) suggests that sizable activation barriers prevent dissociation of the Na−TPA ionic bonds and would explain why additional Na−TPA phases still persist in addition to the α phase even after annealing. This is consistent with our observation that conversion of other phases to the α phase is very slow during extended annealing treatments.

The stability of the structures is likely due, in part, to direct bonding of the TPA to the copper surface. The α phase, as well as other observed phases, has a Na:TPA ratio of 1:1, which means that for each +1 charge cation, there are two −1 charge carboxylate moieties. The carboxylate units most likely still have a significant bond to Cu, some part of what they experience on Cu in the absence of Na, as discussed previously.[28,47] Compared to gas phase, ionic structures at metal surfaces will certainly experience some weaker forces due to surface screening of the adsorbed charges. However, experimental evidence shows (vide supra) that the interactions strengths are still significant enough to stabilize the network at elevated temperature. It is possible that the TPA−Cu bonding compensates for whatever weakening of the ionic bonds occurs at the copper surface (due to screening of the electrostatic interaction, for example). Previous studies of Cs−TPA found a 1:4 cation:anion ratio due to the large size of the cation.[13] Compared to the present case, that study observed a lower stability in the ionic structure, likely due to the 1:4 ratio and charge imbalance.

The temperature of the sample was increased to more than 180 °C for 12 h to rigorously test the thermal stability of the organic building block. After samples were annealed in excess of 200 °C for 5 min, no noticeable degradation in STM structures or XPS data was evident. However, very slow decomposition of TPA molecules was observed after annealing for many hours, chiefly manifested as a decarboxylation from the scission of a

carbon−carbon bond in XPS data. The decomposition of TPA on a Cu(100) surface occurs after annealing at 180 °C with or without the presence of NaCl. After an extended (15 h) 180 °C anneal, there is a 42% decrease in the O 1s XPS peak area and a 34% decrease in the C 1s feature associated with the carboxylate group (see Figure S4). Notably, the C 1s peak associated with the aromatic carbons of TPA does not decrease after annealing. The substantial decrease in oxygen and carboxylate carbon indicates decarboxylation of the molecule and desorption of CO_2 from the surface. Indeed, the evolution of CO_2 gas (mass 44) from the surface was detected using a mass spectrometer as the sample was heated. The observed changes in XPS peak areas and evolution of CO_2 gas are consistent with prior work regarding first-layer decomposition of TPA, which was said to proceed via a decarboxylation mechanism.[25]

The observation that the C−C bond between the terephthalate and the aromatic ring can break at 180 °C, even though the ionic bond between the negatively charged carboxylate groups in TPA and Na ions on the Cu(100) surface remains intact at 165 °C, suggests that these bonds are similar in strength. Indeed, the binding energy between two ions is similar to the energy of a covalent bond in vacuum when no solvent of a high dielectric constant is present.[20] These results provide the first evidence of the comparability of ionic and covalent bond strengths in ionic nanostructures at the metallic surface.

CONCLUSIONS

Very high thermal stability of an organic ionic structure self-assembled at a surface with atomic precision has been achieved, as shown by high-temperature STM data. Self-assembly occurs by interaction of carboxylate groups with alkali metal cations and is enabled by use of a reactant (NaCl) that is cheap, safe, and easy to work with. Structures partake in cooperative interactions to achieve stability, benefitting both from strong ionic interactions between adsorbates as well as metal−organic chemisorption bonds to the surface. Sodium-carboxylate ionic structures maintain their atomic organization when imaged with molecular resolution at 165 °C. Disruption of the self-assembled supramolecular networks at 180 °C occurs due to the scission of intramolecular covalent bonds in the organic building block. We show that intermolecular ionic and intramolecular covalent interactions can be comparable in strength in self-assembled nanostructures at metal surfaces. This result provides a valuable design consideration for future surface systems and demonstrates that screening effects of the metallic surface can be overcome by cooperative interactions. Robust nanostructures formed by hybrid ionic self-assembly at surfaces are promising for applications that require atomic precision in structural organization in addition to great thermal stability and resistance to unwanted interfacial diffusion.

METHODS

Experiments were conducted in an ultrahigh vacuum (UHV) system of base pressure $<5 \times 10^{-10}$ Torr. A Cu(100) single-crystal surface was cleaned by cycles of argon ion sputtering for 10−14 min at a sample temperature of 200 °C and annealing. The sample was annealed to 480 °C after each sputtering step, except for the final cleaning cycle annealing at 420 °C to obtain large copper terraces. Surface cleanliness was verified by XPS analysis of C 1s and O 1s regions as well as by STM. TPA was vapor deposited onto the Cu(100) surface from a quartz, Knudsen-type evaporator at a crucible temperature of 140 °C.

The surface coverage was controlled by the shutter open time. NaCl was deposited from alumina or quartz crucibles in an electron beam evaporator.

The STM microscope (RHK Technologies) is located in a separate but connected vacuum chamber and was operated at room temperature or elevated temperatures to obtain topographic images of the surface. A sharp tungsten STM tip was fabricated using an electrochemical etching method. Field emission treatments and voltage pulses were used as tip-cleaning procedures in UHV. Bias voltages from 0.5 to 1.7 V and set point currents from 0.2 to 1.2 nA were generally used. The higher bias voltages (above ∼1.0 V) were required for high-quality imaging of surfaces with NaCl. The previously studied structure of self-assembled TPA islands with a (3 × 3) structure on Cu(100) was used for STM image calibration. STM image analysis was done with the WSxM software.[48]

XPS experiments were conducted with a commercial dual anode Mg/Al X-ray source (XR-50, SPECS GmbH) and energy analyzer (PHOIBOS 150, SPECS GmbH), and spectral analysis was done with SpecsLab2 and CasaXPS software. Linear background subtraction was performed on all XPS photoelectron peaks. All XPS peak areas were corrected for transmission factor, the mean free path of the electrons, and relative sensitivity factors. XPS peak positions were corrected for the work function of the energy analyzer, using the Cu $2p_{3/2}$ binding energy at 932.7 eV.[34] Changes in peak area intensities between experiments were quantified by calculating ratios to the Cu $2p^{3/2}$ peak area. Thermal desorption experiments were conducted by cooling the sample with nitrogen to −185 °C prior to deposition. Desorption events were observed with a Hiden mass spectrometer (HAL 7 RC).

ASSOCIATED CONTENT

Ⓢ Supporting Information

Additional information regarding the surface reaction, ionic structures, and high temperature stability are provided. This information is available free of charge via the Internet at http://pubs.acs.org.

AUTHOR INFORMATION

Corresponding Author

tait@indiana.edu

Notes

The authors declare no competing financial interest.

ACKNOWLEDGMENTS

REFERENCES

(1) Barth, J. V.; Costantini, G.; Kern, K. Nature 2005, 437 (7059), 671−679.
(2) Schreiber, F. Prog. Surf. Sci. 2000, 65 (5−8), 151−256.
(3) Langner, A.; Tait, S. L.; Lin, N.; Chandrasekar, R.; Ruben, M.; Kern, K. Angew. Chem., Int. Ed. 2008, 47 (46), 8835−8838.
(4) Barth, J. V. Surf. Sci. 2009, 603 (10−12), 1533−1541.
(5) Barth, J. V. Annu. Rev. Phys. Chem. 2007, 58, 375−407.
(6) Bartels, L. Nat. Chem. 2010, 2 (2), 87−95.
(7) Smith, R. K.; Lewis, P. A.; Weiss, P. S. Prog. Surf. Sci. 2004, 75 (1−2), 1−68.
(8) Grossiord, N.; Kroon, J. M.; Andriessen, R.; Blom, P. W. M. Org. Electron. 2012, 13 (3), 432−456.
(9) Rosch, R.; Tanenbaum, D. M.; Jorgensen, M.; Seeland, M.; Barenklau, M.; Hermenau, M.; Voroshazi, E.; Lloyd, M. T.; Galagan, Y.; Zimmermann, B.; Wurfel, U.; Hosel, M.; Dam, H. F.; Gevorgyan, S. A.; Kudret, S.; Maes, W.; Lutsen, L.; Vanderzande, D.; Andriessen, R.; Teran-Escobar, G.; Lira-Cantu, M.; Rivaton, A.; Uzunoglu, G. Y.; Germack, D.; Andreasen, B.; Madsen, M. V.; Norrman, K.; Hoppe, H.; Krebs, F. C. Energ. Environ. Sci. 2012, 5 (4), 6521−6540.

(10) De Feyter, S.; De Schryver, F. C. *Chem. Soc. Rev.* **2003**, *32* (6), 393−393.

(11) Payer, D.; Comisso, A.; Dmitriev, A.; Strunskus, T.; Lin, N.; Woll, C.; DeVita, A.; Barth, J. V.; Kern, K. *Chem.—Eur. J.* **2007**, *13* (14), 3900−3906.

(12) Lackinger, M.; Heckl, W. M. *J. Phys. D: Appl. Phys.* **2011**, *44* (46), 464011.

(13) Stepanow, S.; Ohmann, R.; Leroy, F.; Lin, N.; Strunskus, T.; Woll, C.; Kern, K. *ACS Nano* **2010**, *4* (4), 1813−1820.

(14) Meng, R. P.; Xu, H. G.; Xu, C. X.; Zhang, J. X.; He, G. H.; Cui, Y. P. *Chin. Phys. Lett.* **2003**, *20* (6), 935−937.

(15) Vetriani, C.; Maeder, D. L.; Tolliday, N.; Yip, K. S. P.; Stillman, T. J.; Britton, K. L.; Rice, D. W.; Klump, H. H.; Robb, F. T. *P. Natl. Acad. Sci. U.S.A.* **1998**, *95* (21), 12300−12305.

(16) Zhu, Z. H.; Daniel, T. A.; Maitani, M.; Cabarcos, O. M.; Allara, D. L.; Winograd, N. *J. Am. Chem. Soc.* **2006**, *128* (42), 13710−13719.

(17) Xu, W.; Wang, J. G.; Yu, M.; Laegsgaard, E.; Stensgaard, I.; Linderoth, T. R.; Hammer, B.; Wang, C.; Besenbacher, F. *J. Am. Chem. Soc.* **2010**, *132* (45), 15927−15929.

(18) Jung, T. A.; Wackerlin, C.; Iacovita, C.; Chylarecka, D.; Fesser, P.; Ballav, N. *Chem. Commun.* **2011**, *47* (32), 9146−9148.

(19) Krebs, R. E. *The History and Use of our Earth's Chemical Elements: A Reference Guide*, 2nd ed.; Greenwood Press: Westport, CT, 2006.

(20) Israelachvili, J. N. *Intermolecular and Surface Forces*, 3rd ed.; Academic Press: Burlington, MA, 2011.

(21) Robertson, N. *Angew. Chem., Int. Ed.* **2006**, *45* (15), 2338−2345.

(22) Nattestad, A.; Mozer, A. J.; Fischer, M. K. R.; Cheng, Y. B.; Mishra, A.; Bauerle, P.; Bach, U. *Nat. Mater.* **2010**, *9* (1), 31−35.

(23) Katono, M.; Bessho, T.; Meng, S.; Humphry-Baker, R.; Rothenberger, G.; Zakeeruddin, S. M.; Kaxiras, E.; Gratzel, M. *Langmuir* **2011**, *27* (23), 14248−14252.

(24) Sepehrifard, A.; Stublla, A.; Haftchenary, S.; Chen, S. G.; Potvin, P. G.; Morin, S. *J. New Mater. Electrochem. Syst.* **2008**, *11* (4), 281−285.

(25) Martin, D. S.; Cole, R. J.; Haq, S. *Phys. Rev. B* **2002**, *66* (15), 155427.

(26) Pranger, L.; Tannenbaum, R. *J. Colloid Interface Sci.* **2005**, *292* (1), 71−78.

(27) Zasada, F.; Piskorz, W.; Godlewski, S.; Prauzner-Bechcicki, J. S.; Tekiel, A.; Budzioch, J.; Cyganik, P.; Szymonski, M.; Sojka, Z. *J. Phys. Chem. C* **2011**, *115* (10), 4134−4144.

(28) Ge, Y.; Adler, H.; Theertham, A.; Kesmodel, L. L.; Tait, S. L. *Langmuir* **2010**, *26* (21), 16325−16329.

(29) Stepanow, S.; Strunskus, T.; Lingenfelder, M.; Dmitriev, A.; Spillmann, H.; Lin, N.; Barth, J. V.; Woll, C.; Kern, K. *J. Phys. Chem. B* **2004**, *108* (50), 19392−19397.

(30) Bennewitz, R.; Foster, A. S.; Kantorovich, L. N.; Bammerlin, M.; Loppacher, C.; Schar, S.; Guggisberg, M.; Meyer, E.; Shluger, A. L. *Phys. Rev. B* **2000**, *62* (3), 2074−2084.

(31) Guo, Q. M.; Qin, Z. H.; Liu, C. D.; Zang, K.; Yu, Y. H.; Cao, G. Y. *Surf. Sci.* **2010**, *604* (19−20), 1820−1824.

(32) Olsson, F. E.; Persson, M. *Surf. Sci.* **2003**, *540* (2−3), 172−184.

(33) Kishi, K.; Miyoshi, H. *J. Electron. Spectrosc.* **1991**, *53* (4), 237−249.

(34) Moulder, J. F.; Chastain, J. *Handbook of X-ray Photoelectron Spectroscopy: A Reference Book of Standard Spectra for Identification and Interpretation of XPS data*; Physical Electronics Division, Perkin-Elmer Corp.: Eden Prairie, MN, 1992.

(35) Vickerman, J. C.; Gilmore, I. S., *Surface Analysis: The Principal Techniques*, 2nd ed.; Wiley: Chichester, U.K., 2009.

(36) Nakakura, C. Y.; Phanse, V. M.; Altman, E. I. *Surf. Sci.* **1997**, *370* (1), L149−L157.

(37) Walter, W. K.; Manolopoulos, D. E.; Jones, R. G. *Surf. Sci.* **1996**, *348* (1−2), 115−132.

(38) Dmitriev, A.; Lin, N.; Weckesser, J.; Barth, J. V.; Kern, K. *J. Phys. Chem. B* **2002**, *106* (27), 6907−6912.

(39) Lin, N.; Dmitriev, A.; Weckesser, J.; Barth, J. V.; Kern, K. *Angew. Chem., Int. Ed.* **2002**, *41* (24), 4779−4783.

(40) Tseng, T. C.; Urban, C.; Wang, Y.; Otero, R.; Tait, S. L.; Alcami, M.; Ecija, D.; Trelka, M.; Gallego, J. M.; Lin, N.; Konuma, M.; Starke, U.; Nefedov, A.; Langner, A.; Woll, C.; Herranz, M. A.; Martin, F.; Martin, N.; Kern, K.; Miranda, R. *Nat. Chem.* **2010**, *2* (5), 374−379.

(41) Tseng, T.-C.; Abdurakhmanova, N.; Stepanow, S.; Kern, K. *J. Phys. Chem. C* **2011**, *115* (20), 10211−10217.

(42) Clair, S.; Pons, S.; Fabris, S.; Baroni, S.; Brune, H.; Kern, K.; Barth, J. V. *J. Phys. Chem. B* **2006**, *110* (11), 5627−5632.

(43) Suleiman, I. A.; Radny, M. W.; Gladys, M. J.; Smith, P. V.; Mackie, J. C.; Kennedy, E. M.; Dlugogorski, B. Z. *Phys. Chem. Chem. Phys.* **2011**, *13* (21), 10306−10311.

(44) *CRC Handbook of Chemistry and Physics*, 92nd ed.; Haynes, W. M., Ed.; CRC Press: Boca Raton, FL, 2011-2012; http://www.hbcpnetbase.com/.

(45) Kaduk, J. A. *Acta Crystallogr., Sect. B* **2000**, *56*, 474−485.

(46) Koczkur, K. M.; Hamed, E. M.; Houmam, A. *Langmuir* **2011**, *27* (20), 12270−12274.

(47) Tait, S. L.; Lim, H.; Theertham, A.; Seidel, P. *Phys. Chem. Chem. Phys.* **2012**, *14*, 8217−8223.

(48) Horcas, I.; Fernandez, R.; Gomez-Rodriguez, J. M.; Colchero, J.; Gomez-Herrero, J.; Baro, A. M. *Rev. Sci. Instrum.* **2007**, *78* (1), 013705.